Nano LIFE
Vol. 2, No. 2 (2012) 1230007 (14 pages)

DOI: 10.1142/S1793984411000517

World Scientific
www.worldscientific.com

COMPUTATIONAL SIMULATIONS OF NANOSTRUCTURED SOLAR CELLS

BAOMIN WANG, TONGCHUAN GAO and PAUL W. LEU
Department of Industrial Engineering
University of Pittsburgh
Pittsburgh, PA, 15261, USA

Revised 1 February 2012
Accepted 17 February 2012
Published 11 May 2012

Simulation methods are vital to the development of next-generation solar cells such as plasmonic, organic, nanophotonic, and semiconductor nanostructure solar cells. Simulations are predictive of material properties such that they may be used to rapidly screen new materials and understand the physical mechanisms of enhanced performance. They can be used to guide experiments or to help understand results obtained in experiments. In this paper, we review simulation methods for modeling the classical optical and electronic transport properties of nanostructured solar cells. We discuss different techniques for light trapping with an emphasis on silicon nanostructures and silicon thin films integrated with nanophotonics and plasmonics.

Keywords: Photovoltaics; light trapping; plasmonic; silicon; nanophotonic.

1. Introduction

Solar power is an attractive energy resource because it is renewable and abundant. It is also relatively free of problems associated with fossil fuels or nuclear energy, such as increasing fuel costs, waste disposal, heat dissipation, safety concerns, and the release of greenhouse gases. The solar cell industry is about $50 billion dollars and growing over 40% annually.[1] Photovoltaic systems are also modular and may be installed near points of use and put on line quickly as the demand for electricity increases. Solar power has great potential in helping provide electricity to the approximately 1.6 billion people or about a quarter of humanity that are currently without electricity.[2] Millions of small villages around the world could rely on solar energy to provide power for water, refrigeration, sanitation, communication, and universal education.[3,4] While photovoltaic cells have steadily made improvements in efficiency,[5,6] significant improvements in device performance and manufacturing processes are needed for more widespread adoption. The cost per efficiency of solar cells must *decrease dramatically*, by approximately 5−10 times to compete with fossil and nuclear electricity and by a factor of 25−50 to compete with primary fossil energy.[7]

Advances in nanotechnology are helping address these challenges in solar cells through the development of new low-cost materials and architectures with superior optical and electronic properties. New scalable manufacturing methods have been developed that allow for these materials to be manufactured inexpensively over large areas. Tremendous progress has also been made into characterizing the fundamental interactions of light with matter at the nanoscale and carrier transport processes. Advances

in nanotechnology have led to significant developments in plasmonic solar cells,[8–10] dye-sensitized photovoltaics,[11–15] organic solar cells,[16–19] nanostructured semiconductor solar cells,[20,21] photonic crystals,[22,23] and transparent conductors.[24–27] Nanostructures have the potential to substantially decrease manufacturing costs while maintaining reasonable power conversion efficiencies. They enable the use of less material and poorer quality material since electron-hole pairs or excitons do not need to travel as far to be collected. Nanostructures may be deposited on low-cost substrates such as glass or plastics by chemical vapor deposition directly[31–33] or transferred after growth.[34–36] For transparent conductors, nanomaterials such as carbon nanotube films,[25,37–42] graphene films,[24,43–49] and random networks of metallic nanowires[26,28,50] have been demonstrated as low sheet resistance, high transmission materials. Furthermore, while thin films are brittle, these nanomaterials are strong and suitable for flexible photovoltaics.[34,51]

The role of computational tools are critically important in the development of nanostructured solar cells. As computational power rapidly increases, large-scale problems may be addressed and many different materials and geometries may be quickly screened. Theoretical simulation tools have played an integral part in understanding and designing nanostructured solar cells. Computations can be made *ab initio* (without assumptions or simplifications), and are *predictive* of material properties such that they can be used to suggest new and better structures. Simulated absorption, reflection, and transmission spectra have consistently agreed with experimental results. Photonic structure, local electric field-intensity, and local current generation simulations may be used to elucidate the mechanisms for enhanced performance and help understand

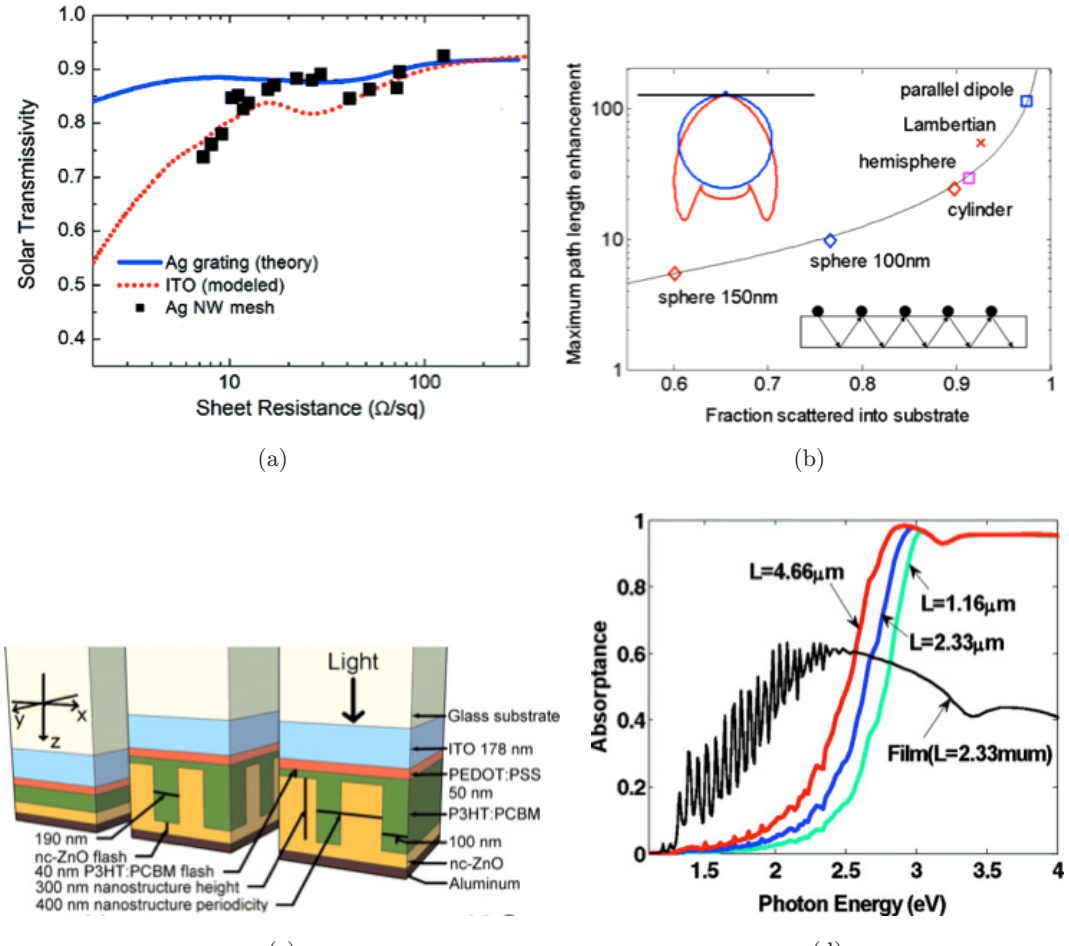

Fig. 1. Simulations have proven to be integral to understanding and improving nanostructures for (a) transparent conductors,[28] (b) plasmonic solar cells,[8] (c) organic solar cells,[29] and (d) silicon nanowires.[30]

experimental results. Angle-dependent simulations are also useful for evaluating the absorption of sunlight that a nontracking photovoltaic device would be expected to exhibit over an average day. Figure 1 highlights some of the innovations in nanostructured photovoltaics systems that have been studied through simulations. Two physical processes may be modeled: the interaction of light with the nanomaterial and the electrical transport of photogenerated carriers. In this paper, we review different methods for the modeling of these nanostructures for solar cells as highlighted by silicon-based photovoltaics.

2. Silicon as a Solar Material

Silicon is promising as a low-cost, high-efficiency photovoltaic material. Silicon is a naturally abundant, stable, nontoxic material that has been used extensively for integrated circuits, so that its processing and manufacturing is well developed. Crystalline silicon currently represents about 90% of the photovoltaic market. The band gap of crystalline silicon is 1.12 eV, which has a maximum detailed balance limit of $\eta = 33.2\%$ as shown in Fig. 2. This efficiency is nearly optimal for capturing the solar spectrum. The maximum efficiency, calculated from the global 37° tilt Air Mass 1.5 (AM1.5) spectrum[52] while considering radiative recombination through spontaneous emission, is also known as the Shockley–Queisser limit.[53]

However, the main challenge with the use of silicon for photovoltaics is that silicon is not a strong

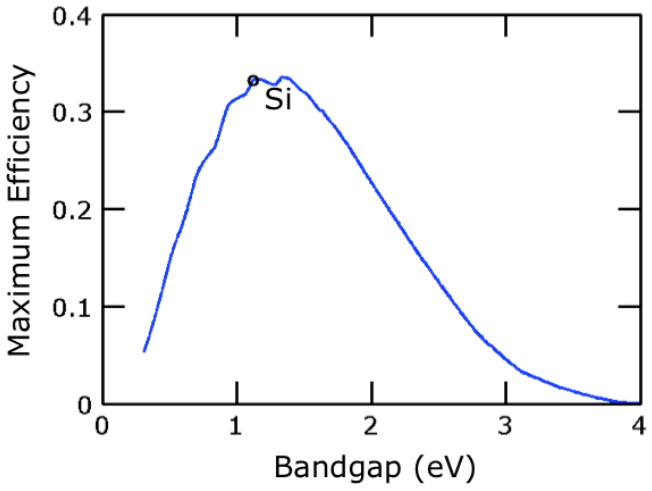

Fig. 2. Maximum theoretical conversion efficiency versus energy band gap for solar cells in AM1.5 sunlight. The maximum efficiency for crystalline silicon is 33.2%.

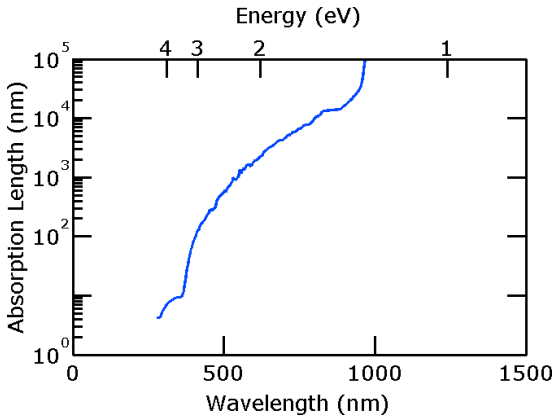

Fig. 3. Absorption length of silicon versus wavelength.

absorber of sunlight in the near-infrared region. Silicon is an indirect band gap material and thus the edge of the absorption coefficient is not sharp. Photons with energy just above the silicon band gap require phonon interactions for absorption and thus, their probability of absorption is lower. Figure 3 shows the absorption length of crystalline silicon as a function of wavelength.[54] Silicon has absorption lengths $L_\alpha > 10\,\mu$m for photons with $\lambda > 800$ nm and $L_\alpha > 100\,\mu$m for $\lambda > 970$ nm.

Conventional silicon photovoltaics are thus typically of thicknesses $200-300\,\mu$m to ensure the absorption of most sunlight. However, single crystalline silicon solar cells require expensive manufacturing methods, such as the Siemens method for solar grade purification, Czochralski method for crysallization, and wafer slicing. The silicon must be of high quality to allow for electrons and holes to diffuse through the material and be collected with high quantum efficiency. There are also additional costs associated with supporting the weight of this material.

Different light trapping strategies are thus important for increasing the photon optical length, the distance a photon travels in silicon before escaping, in order to increase absorption for a particular thickness of silicon. Light trapping with sub-wavelength nanostructures involves coupling light into localized resonant modes and guided resonance modes in the active region to increase absorption. Nanophotonic light trapping strategies have used structuring of the silicon itself or patterning of dielectric materials on the front and back of the silicon. Plasmonic light trapping has involved using different metal nanostructures on the back and front

of the active region to increase absorption. Light trapping allows for not only the use of less silicon but also poorer quality silicon (such as amorphous or poly-crystalline silicon) with shorter minority carrier diffusion lengths since electron-hole pairs are generated closer to the internal electric field. Open circuit voltages are increased due to improved carrier collection while material costs are decreased.

3. Experimentally Fabricated Solar Cells

Sunlight can provide at most about $1\,\mathrm{kW/m^2}$ of power. Thus, large areas are required for photovoltaics to generate adequate amounts of power, and material and processing issues are important as they determine the costs associated with the solar cell. *Scalable manufacturing methods* are critical for assembling nanostructures cheaply, robustly, and precisely over meter-sized areas.

Many innovative silicon structures have been experimentally demonstrated for the active region in solar cells, including ultrathin microcells,[34] crystalline silicon nanowire arrays,[31–33,36,55–59] horizontal silicon nanowire arrays,[60] crystalline silicon single nanowires,[61–63] amorphous nanopillar and nanocone (NC) arrays,[64,65] crystalline silicon nanoholes,[66] and silicon photonic crystals.[67] Nanostructured photovoltaics have utilized bottom-up techniques such as chemical vapor deposition, or a number of top-down methods such as the use of combined Langmuir–Blodgett assembly and reactive ion etching,[65] galvanic displacement reaction,[55] and wet electroless chemical etching.[31] Photonic crystals have also been used next to the silicon active region to enhance absorption by coupling light into guided resonance modes. This has been demonstrated in crystalline silicon,[68] nanocrystalline,[69] and amorphous silicon.[70]

Plasmonic nanostructures have also been experimentally demonstrated as an effective way to increase absorption in silicon. In thin-film silicon photovoltaic cells, metallic nanostructures may utilize plasmons for light trapping by sub-wavelength scattering, coupling to localized surface plasmons, or coupling into propagating surface plasmon polaritons.[10] Most work has focused on the use of metal nanoparticles to enhance light trapping through plasmonic scattering. Metal nanoparticles are strong scatterers of light near their plasmon resonance and may be used to used to scatter light preferentially into a dielectric.[71] Metal nanoparticles have been utilized to enhance optical absorption in single-crystalline Si,[72] amorphous Si,[73–76] and Si-on-insulator[77] photovoltaic cells. The plasmon resonances of Ag and Au nanoparticles have been shown to be shifted by embedding them in SiO_2, Si_3N_4, or Si.[78–80] Locating the nanoparticles on the rear of solar cells can help avoid absorption losses below the resonance wavelength due to interference effects.[78,81,82]

4. Optical Property Simulation Methods

Most simulations have focused on analyzing and improving the solar absorption of the silicon active region. Nanostructured solar cells have feature sizes smaller than the wavelengths of most of the solar spectrum. Geometrical optics is no longer applicable at these length scales and ray-tracing methods are thus, inaccurate. Instead, simulation methods that capture the wave-like nature of light must be utilized such that effects such as interference and diffraction are properly captured. The absorption, transmission, and reflection spectra of most nanomaterials can be predicted from a completely classical theory of electromagnetism. This involves solving Maxwell's equations:

$$\begin{aligned} \nabla \cdot \mathbf{E} &= \frac{\rho}{\epsilon_0} \\ \nabla \cdot \mathbf{B} &= 0 \\ \nabla \times \mathbf{E} &= -\frac{\partial \mathbf{B}}{\partial t} \\ \nabla \times \mathbf{B} &= \mu_0 \mathbf{J} + \mu_0 \epsilon_0 \frac{\partial \mathbf{B}}{\partial t} \end{aligned} \tag{1}$$

where $\mathbf{E}$ and $\mathbf{B}$ are the electric and magnetic fields, and ρ and $\mathbf{J}$ are the free charge and current densities. The materials may be parametrized through phenomenological material parameters such as the complex valued refractive index, $n(\omega) = n_r(\omega) + n_i(\omega)$ or the complex permittivity $\epsilon(\omega) = \epsilon_r(\omega) + \epsilon_i(\omega)$. Simulations agree well with experiments, and typically semiclassical treatments (where light is treated classically and the material is treated quantum mechanically) or full quantum treatments are unnecessary. For example, silicon has a Bohr exciton radius of about 2 nm, such that silicon nanostructure dielectric constants are not modified by quantum mechanics.

A variety of electrodynamic simulation methods have been used in studying the interactions of electromagnetic radiation with nanostructures, including the transfer matrix method (finite difference frequency-domain),[30,83,84] finite element method,[85,86] rigorous coupled mode analysis (fourier modal method),[22,87] and finite difference time-domain (FDTD) methods.[88,89] Electrodynamic simulation methods can be generally classified into time-domain simulations or frequency-domain response methods, and frequency-domain eigensolvers. Common discretization schemes are finite differences, finite elements, and spectral methods.

Finite difference frequency-domain methods such as the transfer matrix method comprise of solving for the electric field $\mathbf{E}(\mathbf{r})\exp^{-i\omega t}$ in terms of the current source $\mathbf{J}(\mathbf{r})\exp^{-i\omega t}$ in Maxwell equations:

$$\left[\left(\nabla\times\nabla-\frac{\omega^2}{c^2}\epsilon(\mathbf{r})\right)\right]\mathbf{E}(\mathbf{r})=i\omega\mu_0\mathbf{J}(\mathbf{r}) \quad (2)$$

The finite difference or finite element method may be applied to this linear equation to discretize it. These equations must be solved for at every frequency, where a table of experimental dielectric constants may be used.

In time domain methods, the full time-dependent Maxwell equations are solved for in both space and time. The most common implementation for time-domain simulations is the finite difference time-domain method (FDTD technique) which divides space and time into a grid of discrete points and approximate the derivatives in Maxwell equations by finite differences.[90] A Yee grid is used in which the different field components are associated with different locations on the grid.[91] Many frequencies can be computed with a single computation, by taking the Fourier transform of the response to a short pulse.

Appropriate boundary conditions can be used to reduce the simulation cell. For example, periodic boundary conditions are used to model semi-infinite arrays. Symmetric and anti-symmetric boundary conditions may also be used to reduce the simulation size. Perfectly matched layers (PMLs) are typically used for certain boundaries of the computational region to ensure that fields radiate to infinity instead of reflecting when they interact with the edge of the simulation cell.[92]

Simulations where the only absorbing material is the active region may use $A(E)=1-R(E)-T(E)$ to calculate the absorption spectra. The ultimate efficiency may be calculated from

$$\eta=\frac{\int_{E_g}^{\infty}I(E)A(E)\frac{E_g}{E}dE}{\int_0^{\infty}I(E)dE}, \quad (3)$$

where E is the photon energy, E_g is the band gap of crystalline silicon, and $I(E)$ is the solar irradiance under the global 37°C tilt Air Mass 1.5 spectrum.[52] The ultimate efficiency describes the efficiency of the cell where each photon absorbed produces one electron-hole pair, and these carriers are collected without recombination such as when the temperature of the cell is 0 K.

In plasmonic solar cells or other architectures that involve other parasitically absorbing materials other than the photoactive active region, the position-dependent absorption must be calculated. The position-dependent absorption per unit volume may be calculated from the divergence of the Poynting vector $\mathbf{P}$:

$$A(\mathbf{r},E)=\frac{1}{2}\text{real}\{\nabla\cdot\mathbf{P}\}=\frac{1}{2}\epsilon_i(E)\frac{E}{\hbar}|\mathbf{E}(\mathbf{r},E)|^2 \quad (4)$$

where $\epsilon_i(E)$ is the imaginary part of the dielectric constant, $\hbar$ is the reduced Planck constant, and $\mathbf{E}(\mathbf{r},E)$ is the energy and position-dependent electric field. In most materials, the imaginary part of the permeability $\mu_i=0$, so there is no dependence on the magnetic field, $\mathbf{H}$. Normalization of this quantity over the incoming radiation power used in the simulation and integration over the volume of active-region silicon yields the photocurrent generating energy-dependent absorption $A(E)$.

Simulations also often evaluate the angle integrated absorption,

$$A_\Omega=\int_0^{2\pi}\int_0^{\frac{\pi}{2}}A_{\text{solar}}(\theta,\phi)\cos\theta\,\sin\theta\,d\theta\,d\phi, \quad (5)$$

where θ is the incident angle and ϕ is the azimuthal angle. Angle-dependent simulations are typically made over the entire range of incident angles θ from 0°C to 90°C, and the entire range of azimuthal angles ϕ from 0°C to 360°C, though structural symmetry can often be used to reduce these ranges. The hemispherically averaged light absorption A_Ω as defined by Eq. (5) may then be compared with the $4n^2$ geometrical light trapping limit, which is often referred to as the Yablonvitch limit[93] or Lambertian limit, since Lambertian surfaces, which scatter light uniformly into all forward angles, may

accomplish this.[94] The angle-dependent simulations are also useful in evaluating the absorption that a non-tracking photovoltaic device would be expected to encounter over an average day from approximately $\theta = -45°C$ at 7:00 am to $\theta = 45°C$ at 7:00 pm.

4.1. *Optical property simulation examples*

Optical simulations have proven to be an integral component to the rapid development and understanding of nanostructured solar cells. Photonic crystals have been used to trap light through a variety of different strategies. Several simulation studies involving structuring the silicon active region into a photonic crystal.[22,28,85,96–98] Numerous simulation papers have studied photonic crystals as high-quality back reflectors for light trapping.[95,99–101] Figure 4 highlights two examples from these nanophotonic approaches. Mallick *et al.* demonstrated that a double-layered photonic crystal of crystalline silicon illustrated in Fig. 4(a) increases the short-circuit current by a factor of three times compared to an equivalent volume of silicon.[22] Bermel *et al.* demonstrated that absorption could be improved though the patterning of a variety of photonic crystals in the back of the silicon thin film.[95] Figure 4(b) illustrates

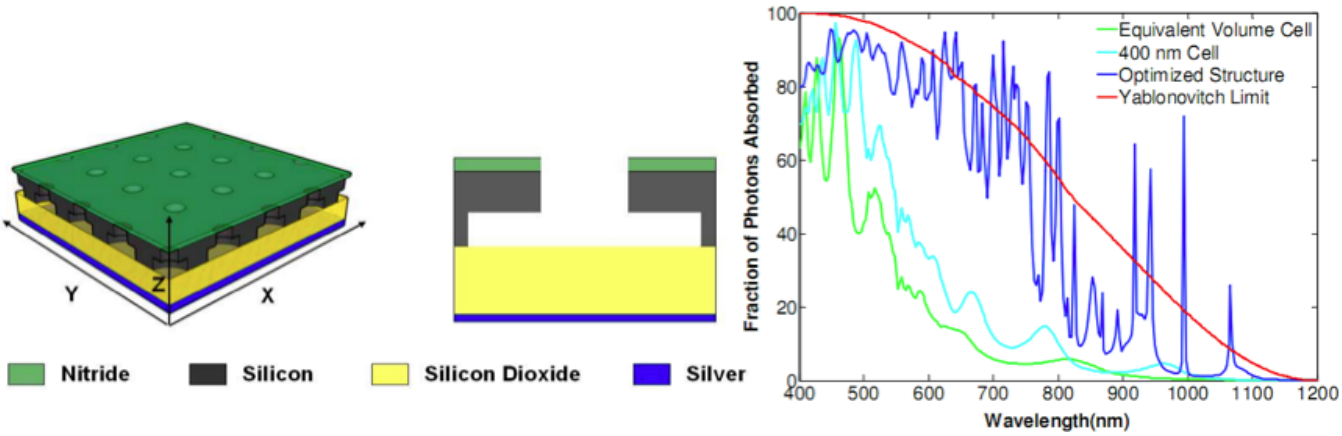

(a)

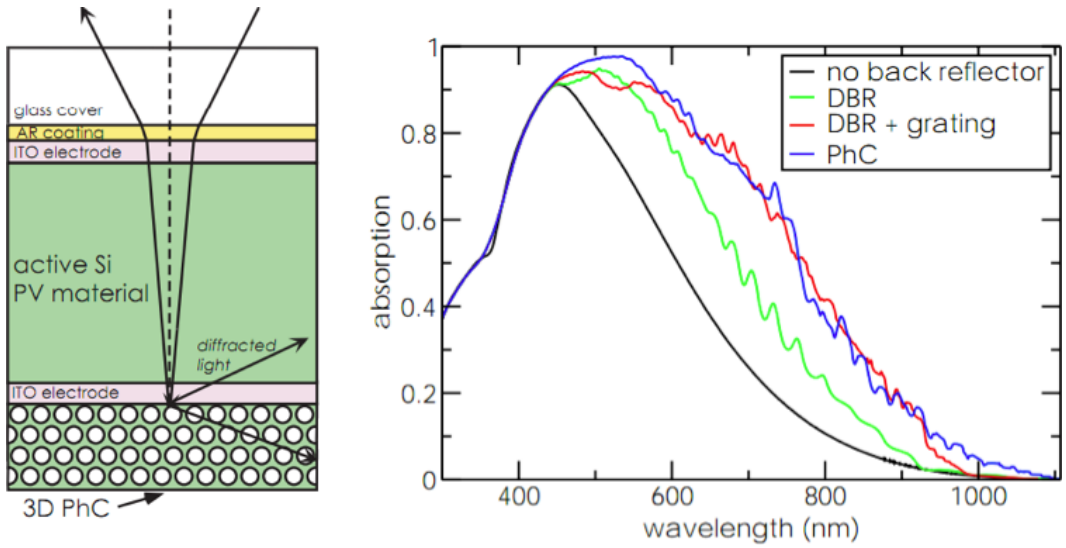

(b)

Fig. 4. New photonic solar cells proposed from simulations. (a) Structuring the silicon itself into a photonic crystal[22] and (b) patterning a photonic crystal next to the silicon.[95]

one of these structures studied, which involves the use of a three-dimensional photonic crystal on the backside of a silicon solar cell.

A number of studies have evaluated plasmonic solar cells. The shape, size, particle material, and dielectric environment of metal nanoparticles have been systematically evaluated in determining the effect of light scattering.[8,102–104] By modifying the geometries of the nanoparticles, the surface plasmon resonances may be tuned to couple light into the silicon active region. Figure 5 illustrates two plasmonic solar cells where metals patterned on the back of the silicon thin film are used to enhance solar absorption. In Fig. 5(a), metals were structured into nanogrooves on the back interface of thin film silicon solar cells that scatter light over a large cone of angles.[9] In Fig. 5(b), a metallic nanograting on the backside of an amorphous thin film silicon solar cell was demonstrated to enhance absorption through Fabry−Perot resonance, surface plasmon polaritons, and planar wave guide coupling.[105] Two-dimensional periodic arrays of metallic nanostructures may also enhance solar absorption through both near-field light concentration and coupling to waveguide modes.[106]

A variety of silicon nanostructures have been studied through simulations. Hu *et al.* evaluated a variety of thin nanostructured silicon cells including pyramids, skewed pyramids, and rods.[84] Fahr *et al.* evaluated randomly textured silicon when this texture was laterally scaled down to nanometer sizes.[107] A number of periodic light-trapping structures such as cylinders, dimples, cones, inverted pyramids with a variety of mosaics have been evaluated.[108] Nanohole arrays have also been proposed as an improved active region.[81,109,110] Nano-cone-hole structures may be a further improvement over nanohole designs.[111] A plethora of studies have evaluated silicon nanowire structures. Different diameter and pitches of silicon nanowires have been investigated through simulations,[30,86,112,113] as well as aperiodicity[113] and structural randomness through random position, diameter, and length.[114]

Recently, we studied silicon nanocone arrays for a variety of geometries and compared them to

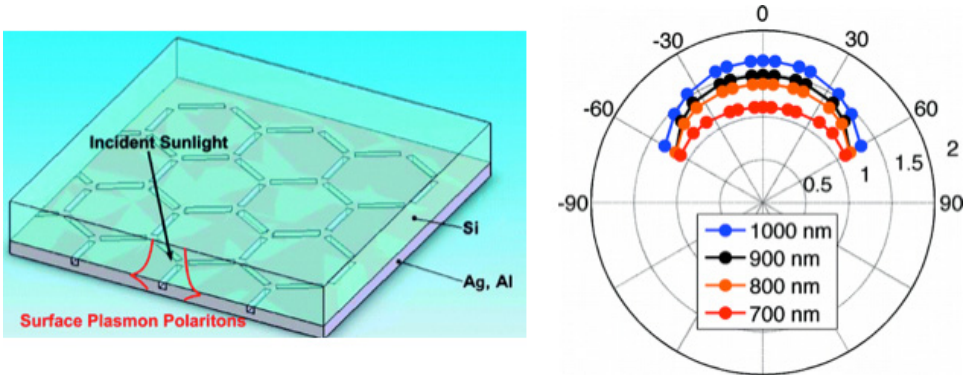

(a)

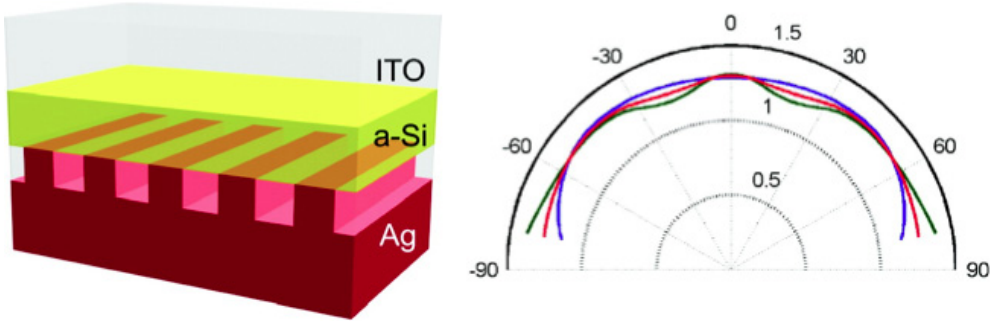

(b)

Fig. 5. New plasmonic solar cells proposed from simulations. (a) Metal nanogrooves on the back surface of a Si thin film and its absorption enhancement over a wide range of angles[9] and (b) 1-dimensional metal grating on the bak of Si thin film and its absorption enhancement over a wide range of angles.[105]

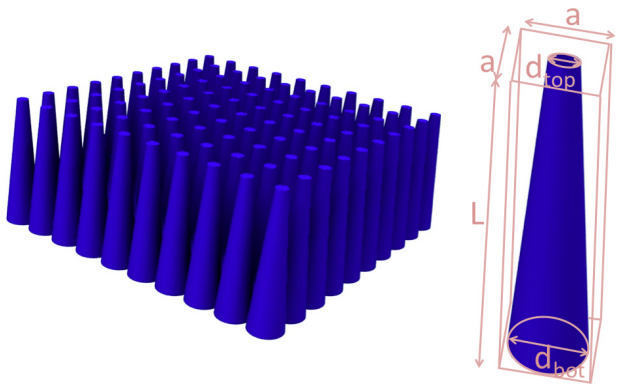

(a) (b)

Fig. 6. (a) Schematic of the silicon nanocone array structure. (b) The parameters for the array are the length L, the period a, the top diameter d_{top}, and the bottom diameter d_{bot}.

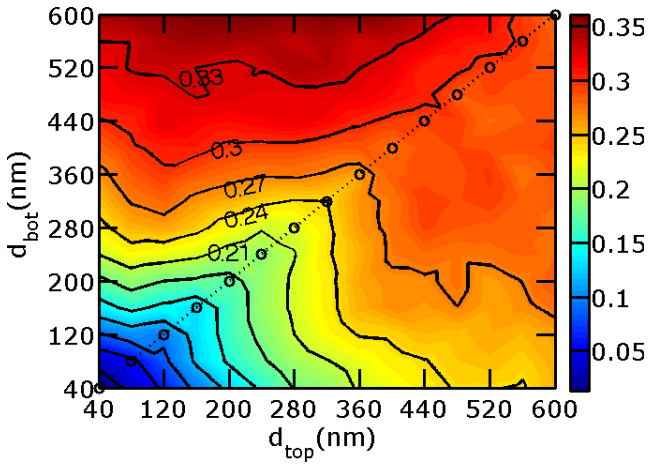

Fig. 7. Ultimate efficiency of silicon nanowires and nanocones where the length $L = 2.33\,\mu$m and pitch $a = 600\,$nm. Contour plot of ultimate efficiency for silicon nanocone arrays as a function of d_{top} and d_{bot}. The dotted line indicates $d_{\text{top}} = d_{\text{bot}}$, which is the geometry of nanowire arrays.

nanowire arrays.[115] We found significant enhancements to absorption and conversion efficiencies in silicon nanocone arrays. Figure 6 shows the schematic of the silicon nanocone arrays studied. The parameters of the structure are the length L, the period a of the square lattice, and the top diameter d_{top} and the bottom diameter d_{bot}. We employed the finite difference time domain method for solving Maxwell's equations.

In our studies, we focused on a variety of different geometries for silicon nanocones with fixed pitch $a = 600\,$nm, since this pitch has been shown to be optimal for silicon nanowires.[86,112] The efficiencies of nanocones and nanowires were compared at a variety of lengths, though we initially focused on nanocones and nanowires with length $L = 2.33\,\mu$m. Figure 7 utilizes a contour plot to illustrate the dependence of ultimate efficiency on the geometry of the silicon nanocone. The parameters d_{top} and d_{bot} were varied from 40 nm to 600 nm in 40 nm increments and values between data points were obtained by triangle-based linear interpolation. Nanowires are special instances of nanocones, where the diameter is constant across the entire length of the structure or $d = d_{\text{top}} = d_{\text{bot}}$, and a dotted line is plotted in the contour plot to indicate this geometry. The optimal ultimate efficiency for nanowire arrays was found to be 29.8% when $d = 560\,$nm or the fill fraction $f = 0.68$. The ultimate efficiency is $> 27\%$ when $d > 400\,$nm (or $f > 0.35$). However, we found that nanocones where $d_{\text{top}} < d_{\text{bot}}$ may be utilized to achieve better ultimate efficiencies than nanowires. The optimal ultimate efficiency was 36.2% for $d_{\text{top}} = 200\,$nm and $d_{\text{bot}} = 600\,$nm, which is about 22% higher than that of the optimal single diameter nanowire array. One of the advantages of nanocones that may be observed from the contour plot is that the ultimate efficiency is not particularly sensitive to d_{top}. For example, ultimate efficiencies greater than 31% may be achieved for nanowires with $d_{\text{bot}} = 600\,$nm and $d_{\text{top}} < 520\,$nm. Optimal nanocone structures are robust in deviations from idealized geometries and not particularly sensitive to variation or imperfections in manufacturing techniques.

Based on the results of our investigations into different nanocone and nanowire geometries, we chose several representative nanowire and nanocone systems to compare their reflection, transmission, and absorption spectra. Figure 8 illustrates the (a) reflection, (b) transmission, and (c) absorption as a function of energy for three representative systems. The optimum efficiency nanowire with $d = 560\,$nm and optimum nanocone with $d_{\text{top}} = 200\,$nm and $d_{\text{bot}} = 600\,$nm are shown. Furthermore, we plot the spectra of the nanowire with $d = 200\,$nm, since this is the top diameter of the optimal nanocone. In Fig. 8(c), the absorption was calculated from $A(E) = 1 - R(E) - T(E)$, and the global 37°C tilt Air Mass 1.5 spectrum is shown on the right y-axis.

Single-diameter nanowire systems exhibit a tradeoff between reflection and transmission. Smaller diameter nanowires such as the one illustrated with $d = 200\,$nm have less reflection because there is less fill factor or area for light to reflect off the top of the

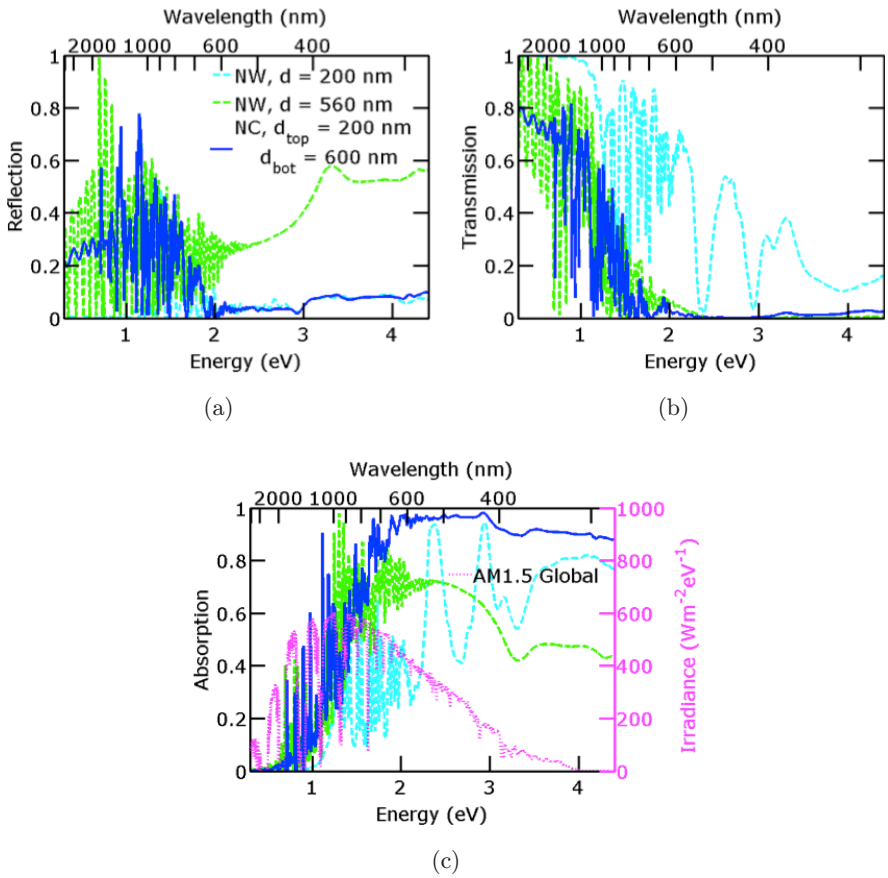

Fig. 8. Optical properties of three different silicon nanostructures: single diameter NW arrays with $d = 200\,\text{nm}$ and $d = 560\,\text{nm}$ and NC arrays with $d_{\text{top}} = 200\,\text{nm}$ and $d_{\text{bot}} = 600\,\text{nm}$. (a), (b), and (c) show the reflectance, transmittance, and absorption respectively. The irradiance of the Air Mass 1.5 solar spectrum is shown in the right y-axis of (c).

nanowires. However, they also have higher transmission throughout the entire solar spectrum because there is less silicon to absorb the light. Smaller diameter nanowires have better absorption in the ultraviolet regime ($> 3.1\,\text{eV}$), but poorer absorption in the infrared regime ($< 1.7\,\text{eV}$). The nanowire array with $d = 200\,\text{nm}$ absorbs 35% of photons above the silicon band gap, 21% in the infrared region (and above the silicon band gap), 67% of photons in the ultraviolet region, and 45% of photons in the visible region. On the other hand, larger diameter nanowire arrays, such as the optimal single diameter system with $d = 560\,\text{nm}$ exhibit higher reflection due to higher fill factor and smaller transmission since there is more material to absorb the light. Larger diameter nanowire arrays have better absorption in the infrared range, but poorer absorption in the ultraviolet range. The nanowire array with $d = 560\,\text{nm}$ absorbs 61% of the photons above the silicon band gap, 52% of photons in the infrared region (and above the silicon band gap), 46% of photons in the ultraviolet region, and 69% of the photons in the visible spectrum.

Silicon nanocone arrays address the tradeoff between reflection and transmission with a smaller d_{top} and a larger d_{bot}. The optimal silicon nanocone array, with $d_{\text{top}} = 200\,\text{nm}$ and $d_{\text{bot}} = 600\,\text{nm}$, especially in the visible and ultraviolet range, has reflection about the same of the small single diameter nanowire array with $d = 200\,\text{nm}$. The larger base results in a transmission that is almost zero in the visible and ultraviolet regime. In the infrared range, the silicon nanocone array has absorption characteristics comparable to that of the best single diameter nanowire array. However, in the visible and ultraviolet range, the absorption is significantly improved with absorption from about 80% to 95% compared to 40−80% for the best single diameter structures. The optimal silicon nanocone array absorbs 74% of photons above the silicon band gap, 54% in the infrared region (above the silicon band gap), 91% in the ultraviolet region, and 93% in the

visible region. Silicon nanocone arrays have enhanced absorption compared to silicon nanowire arrays over the entire spectral range due to antireflection and low transmission in the visible and ultraviolet ranges.

Guided resonance modes (also called leaky-mode resonances) have been shown to play a significant role in light absorption by nanowires.[112,116] Nanowire arrays exhibit a mirror-symmetry plane at $z = 0$, such that modes must be either symmetric or antisymmetric about the plane. TE-like modes are odd with respect to z and TM-like modes are even with respect to z. Distinct peaks may be seen in the absorption spectrum of nanowire arrays corresponding to the coupling of incident light with these guided resonance modes. These guided resonance modes may be tuned for the detection of particular energies or frequencies in photodetectors for example.[116] In photovoltaics however, it is generally desirable for absorption to occur over a broad range of energies. By tapering the nanowires or forming nanocones, the mirror symmetry is removed and the absorption spectrum is broadened such that the overall absorption may be enhanced over that of nanowire arrays.

We considered different geometries of nanocone and nanowire arrays for a wide range of lengths. In addition to the length $L = 2330\,\text{nm}$, we further compared nanocones and nanowires for L from 50 to 10 000 nm for fixed pitch $a = 600\,\text{nm}$. The optimal ultimate efficiency for nanocone and nanowire arrays were obtained from these simulations and plot in Fig. 9. We found that nanocone arrays have better efficiencies than nanowires across a wide range of lengths. The efficiency enhancement of the optimal nanocone array over the nanowire array is plot on the right y-axis in Fig. 9. The ultimate efficiency enhancement is greater than 20% for $L > 500\,\text{nm}$. For the smallest length $L = 50\,\text{nm}$, the amount of silicon is little such that the best structure is a nanowire with $d = a = 600\,\text{nm}$. Most of the loss is through transmission, such that nanocones do not have an advantage over nanowires. However, for longer lengths, nanocones have significant advantages over nanowires when d_{top} is less than d_{bot}. This particular recent study of ours highlights the ability of computational simulations in evaluating different structures and improving their optical absorption properties.

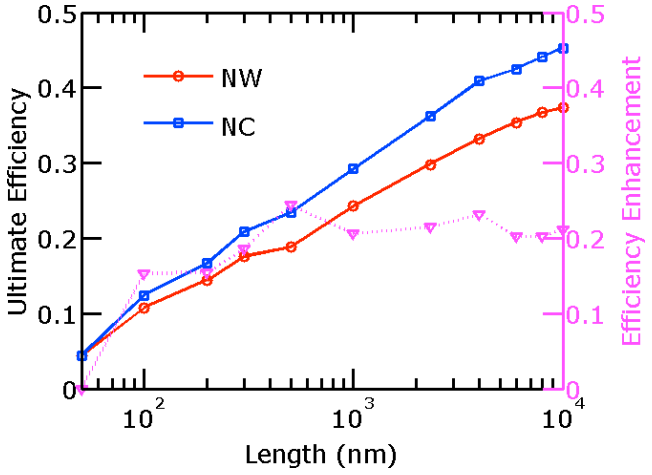

Fig. 9. Optimal ultimate efficiency of silicon nanowires and nanocones with different length L.

5. Transport Simulations

Most solar cell simulations simulate just the optical properties and calculate the ultimate efficiency from the absorption while assuming that that all photogenerated carriers are collected without recombination. This is typically a fairly good approximation, where active regions are small and carriers are collected with high internal quantum efficiency. However, a complete model that includes internal loss mechanisms must also include the electrical transport of photogenerated carriers. Complete simulations have been performed on Ag nanoparticle plasmonic silicon solar cells, where the importance of modeling the electronic transport for low carrier mobility materials was noted.[117] Wang *et al.* have also systematically studied the impact of nanoholes array on the performance of crystalline Si thin film solar cells.[109]

In these studies, the absorption of each photon is assumed to result in an electron-hole pair. The generation rate is thus

$$G(\mathbf{r}, E) = \frac{1}{2E}\,\text{real}\{\nabla \cdot \mathbf{P}\} = \frac{\epsilon_i(E)|\mathbf{E}(\mathbf{r}, E)|^2}{2\hbar}, \quad (6)$$

where $\epsilon_i(E)$ is the imaginary part of the material's permittivity value, $\mathbf{E}(\mathbf{r}, E)$ is the energy and position-dependent electric field. Again, it is assumed the imaginary part of the permeability $\mu_i = 0$, which is true for most solar materials. The photogenerated carrier profile typically expressed in units of $1/(\text{cm}^3\text{s})$ shows the generation of electron-hole pairs at different positions of the solar cell. The generation rate $G(\mathbf{r}, E)$ must be normalized by the

power used in the simulation and then weighted by the power flux density of the solar spectrum in order to obtain the total generation rate $G(\mathbf{r})$.

Transport equations are then solved for under different biases to calculate the photocurrent and dark current. Poisson's equation is solved for at each bias

$$\nabla^2\Phi = -\frac{q}{\epsilon}(p - n + N_{\mathrm{d}} - N_{\mathrm{a}}) - \rho_{\mathrm{trap}}, \qquad (7)$$

where Φ is the electrostatic potential; q is the electron charge; n and p are the electron and hole concentrations, respectively; N_{d} and N_{a} are the impurity concentrations from donors and acceptors respectively; and ρ_{trap} is the charge density from traps and fixed charges. The electron and hole continuity equations are simultaneously solved along with Poisson's equation:

$$\frac{\partial n}{\partial t} = \frac{1}{q}\nabla \cdot \mathbf{J_n} + G - R,$$

$$\frac{\partial p}{\partial t} = -\frac{1}{q}\nabla \cdot \mathbf{J_p} + G - R, \qquad (8)$$

where G is the electron and hole photogeneration rate and R is the electron and hole recombination rate and may include processes such as Auger and Shockley–Read–Hall recombination. The electron and hole currents are

$$\mathbf{J_n}(\mathbf{r}) = -nq\mu_n \nabla\Phi_n,$$

$$\mathbf{J_p}(\mathbf{r}) = -pq\mu_p \nabla\Phi_p, \qquad (9)$$

where μ_n and μ_p are the electron and hole mobilities, and Φ_n and Φ_p are the electron and hole quasi-Fermi potentials, respectively.

Surface recombination in silicon nanostructures is an important consideration due to high surface to volume ratios. Surfaces should be appropriately passivated to reduce recombination rates. Interfacial surface recombination velocity S (typically expressed in cm/sec) is given by

$$S = \sigma v n_{\mathrm{trap}}, \qquad (10)$$

where σ is the capture cross-section, v is the mean thermal velocity, and n_{trap} is the trap state density per unit area. Recombination at the metal contacts may also be considered. It should be noted that low surface recombination velocities $< 10\,\mathrm{cm/s}$ has been reported in oxidized bulk silicon, so that it should be possible to eliminate most of the losses due to surface recombination.[118] By solving the transport equations over a wide range of biases, a complete current–voltage curves under dark and light conditions may be simulated, and the efficiency, fill factor, short circuit current, and open circuit voltage may be obtained. Transport simulations may be used to evaluate different doping profiles, carrier mobility, and carrier recombination mechanisms, and may provide important guidelines for designing nanostructured solar cells.

6. Conclusion

Simulation methods are vital to the development of next-generation solar cells such as plasmonic, organic, nanophotonic, and semiconductor nanostructure solar cells. Simulations are predictive of material properties such that they may be used to rapidly screen new materials and understand experimental results. We reviewed simulation methods for modeling the classical optical and electronic transport properties of nanostructured solar cells and discuss different specific examples of simulations of nanostructured solar cells. In particular, we discuss our recent results on silicon nanocones in more detail. Simulations will continue to be a more integral part of solar cell development as computational power and tools continue to advance.

Acknowledgments

This work was supported by a Mascaro Center for Sustainable Innovation Seed Grant. Computing resources were provided by the Center for Simulation and Modeling at the University of Pittsburgh.

References

1. PV status report 2010.
2. Main message: World Development Report 2010.
3. E. Rosenthal, In Kenya, huts far off the grid harness the sun. *The New York Times*, December 2010.
4. P. Browne, Bringing solar power to Africa's poor. *NYTimes.com*, September 2009.
5. J. Zhao, A. Wang, M. A. Green and F. Ferrazza, *Appl. Phys. Lett.* **73**, 1991 (1998).
6. M. A. Green, K. Emery, Y. Hishikawa and W. Warta, *Progress Photovoltaics: Res. Appl.* **18**, 346 (2010).
7. Basic research needs for solar energy utilization, 2005.
8. K. R. Catchpole and A. Polman, *Appl. Phys. Lett.* **93**, 191113 (2008).

9. V. E. Ferry, L. A. Sweatlock, D. Pacifici and H. A. Atwater, *Nano Lett.* **8**, 4391 (2008).
10. H. A. Atwater and A. Polman, *Nat. Mater.* **9**, 205 (2010).
11. M. Grätzel, *Inorganic Chem.* **44**, 6841 (2005).
12. M. Grätzel, *J. Photochem. Photobiol. C: Photochem. Rev.* **4**, 145 (2003).
13. M. Grätzel, *Nature* **414**, 338 (2001).
14. M. K. Nazeeruddin, F. D. Angelis, S. Fantacci, A. Selloni, G. Viscardi, P. Liska, S. Ito, B. Takeru and M. Grätzel, *J. Am. Chem. Soc.* **127**, 16835 (2005).
15. F. Gao, Y. Wang, D. Shi, J. Zhang, M. Wang, X. Jing, R. Humphry-Baker, P. Wang, S. M. Zakeeruddin and M. Grätzel, *J. Am. Chem. Soc.* **130**, 10720 (2008).
16. H. Hoppe and N. S. Sariciftci, *J. Mater. Res.* **19**, 1924 (2004).
17. Conjugated polymer-based organic solar cells. *Chem. Rev.* **107**, 1324 2007. PMID: 17428026.
18. C. W. Tang, *Appl. Phys. Lett.* **48**, 183 (1986).
19. G. Li, V. Shrotriya, J. Huang, Y. Yao, T. Moriarty, K. Emery and Y. Yang, *Nat. Mater.* **4**, 864 (2005).
20. K. Hara, T. Horiguchi, T. Kinoshita, K. Sayama, H. Sugihara and H. Arakawa, *Solar Energy Mater. Solar Cells* **64**, 115 (2000).
21. P. V. Kamat, *J. Phys. Chem. C* **112**, 18737 (2008).
22. S. B. Mallick, M. Agrawal and P. Peumans, *Opt. Express* **18**, 5691 (2010).
23. J. G. Mutitu, S. Shi, C. Chen, T. Creazzo, A. Barnett, C. Honsberg and D. W. Prather, *Opt. Express* **16**, 15238 (2008).
24. X. Wang, L. Zhi and K. Mullen, *Nano Lett.* **8**, 323 (2008).
25. T. M. Barnes, X. Wu, J. Zhou, A. Duda, J. van de Lagemaat, T. J. Coutts, C. L. Weeks, D. A. Britz and P. Glatkowski, *Appl. Phys. Lett.* **90**, 243503 (2007).
26. L. Hu, H. S. Kim, J. Lee, P. Peumans and Y. Cui, *ACS Nano* **4**, 2955 (2010).
27. A. Kumar and C. Zhou, *ACS Nano* **4**, 11 (2010).
28. Y. Lee, C. Huang, J. Chang and M. Wu, *Opt. Express* **16**, 7969 (2008).
29. J. R. Tumbleston, D. Ko, E. T. Samulski and R. Lopez, *Appl. Phys. Lett.* **94**, 043305 (2009).
30. L. Hu and G. Chen, *Nano Lett.* **7**, 3249 (2007).
31. V. Sivakov, G. Andrä, A. Gawlik, A. Berger, J. Plentz, F. Falk and S. H. Christiansen, *Nano Lett.* **9**, 1549 (2009).
32. L. Tsakalakos, J. Balch, J. Fronheiser, B. A. Korevaar, O. Sulima and J. Rand, *Appl. Phys. Lett.* **91**(23), 233117 (2007).
33. T. H. Stelzner, M. Pietsch, G. Andrä, F. Falk, E. Ose and S. Christiansen, *Nanotechnology* **19**, 295203 (2008).
34. J. Yoon, A. J. Baca, S. Park, P. Elvikis, J. B. Geddes, L. Li, R. H. Kim, J. Xiao, S. Wang, T. Kim, M. J. Motala, B. Y. Ahn, E. B. Duoss, J. A. Lewis, R. G. Nuzzo, P. M. Ferreira, Y. Huang, A. Rockett and J. A. Rogers, *Nat. Mater.* **7**, 907 (2008).
35. J. M. Spurgeon, K. E. Plass, B. M. Kayes, B. S. Brunschwig, H. A. Atwater and N. S. Lewis, *Appl. Phys. Lett.* **93**, 032112 (2008).
36. K. E. Plass, M. A. Filler, J. M. Spurgeon, B. M. Kayes, S. Maldonado, B. S. Brunschwig, H. A. Atwater and N. S. Lewis, *Adv. Mater.* **21**, 325 (2009).
37. E. M. Doherty, S. De, P. E. Lyons, A. Shmeliov, P. N. Nirmalraj, V. Scardaci, J. Joimel, W. J. Blau, J. J. Boland and J. N. Coleman, *Carbon* **47**, 2466 (2009).
38. M. Kaempgen and G. S. Duesberg and S. Roth, *Appl. Surf. Sci.* **252**, 425 (2005).
39. B. Dan, G. C. Irvin and M. Pasquali, *ACS Nano* **3**(4), 835 (2009).
40. Z. Wu, Z. Chen, X. Du, J. M. Logan, J. Sippel, M. Nikolou, K. Kamaras, J. R. Reynolds, D. B. Tanner, A. F. Hebard and A. G. Rinzler, *Science* **305**, 1273 (2004).
41. L. Hu, D. S. Hecht and G. Grüner, *Nano Lett.* **4**, 2513 (2004).
42. L. Hu, D. S. Hecht and G. Grüner, *Appl. Phys. Lett.* **94**, 081103 (2009).
43. S. De, P. J. King, M. Lotya, A. O'Neill, E. M. Doherty, Y. Hernandez, G. S. Duesberg and J. N. Coleman, *Small* **6**, 458 (2010).
44. S. Bae, H. Kim, Y. Lee, X. Xu, J.-S. Park, Y. Zheng, J. Balakrishnan, T. Lei, H. R. Kim, Y. I. Song, Y.-J. Kim, K. S. Kim, B. Ozyilmaz, J.-H. Ahn, B. H. Hong and S. Iijima, *Nat. Nano* **5**, 574 (2010).
45. H. A. Becerril, J. Mao, Z. Liu, R. M. Stoltenberg, Z. Bao and Y. Chen, *ACS Nano* **2**, 463 (2008).
46. W. Wu, D. Dey, O. G. Memis, A. Katsnelson and H. Mohseni, *Nanoscale Res. Lett.* **3**, 351 (2008).
47. G. Eda, G. Fanchini and M. Chhowalla, *Nat. Nano* **3**, 270 (2008).
48. Y. Wang, X. Chen, Y. Zhong, F. Zhu and K. P. Loh, *Appl. Phys. Lett.* **95**, 063302 (2009).
49. V. C. Tung, L.-M. Chen, M. J. Allen, J. K. Wassei, K. Nelson, R. B. Kaner and Y. Yang, *Nano Lett.* **9**, 1949 (2009).
50. S. De, T. M. Higgins, P. E. Lyons, E. M. Doherty, P. N. Nirmalraj, W. J. Blau, J. J. Boland and J. N. Coleman, *ACS Nano* **3**, 1767 (2009).
51. Z. Fan, H. Razavi, J. won Do, A. Moriwaki, O. Ergen, Y.-L. Chueh, P. W. Leu, J. C. Ho, T. Takahashi, L. A. Reichertz, S. Neale, K. Yu, M. Wu, J. W. Ager and A. Javey, *Nat. Mater.* **8**, 648 (2009).
52. Solar spectral irradiance: Air mass 1.5, National Renewable Energy Laboratory, Renewable

resource Data Center, http://rredc.nrel.gov/solar/spectra/am0/.
53. W. Shockley and H. J. Queisser, *J. Appl. Phys.* **32**, 510 (1961).
54. E. D. Palik, *Handbook of Optical Constants of Solids* (Academic Press, 1997).
55. K. Peng, Y. Xu, Y. Wu, Y. Yan, S. Lee and J. Zhu, *Small* **1**, 1062 (2005).
56. E. C. Garnett and P. Yang, *J. Am. Chem. Soc.* **130**, 9224 (2008).
57. E. Garnett and P. Yang, *Nano Lett.* **10**, 1082 (2010).
58. O. Gunawan and S. Guha, *Solar Energy Mater. Solar Cells* **93**, 1388 (2009).
59. M. D. Kelzenberg, S. W. Boettcher, J. A. Petykiewicz, D. B. Turner-Evans, M. C. Putnam, E. L. Warren, J. M. Spurgeon, R. M. Briggs, N. S. Lewis and H. A. Atwater, *Nat. Mater.* **9**, 239 (2010).
60. L. Cao, P. Fan, A. P. Vasudev, J. S. White, Z. Yu, W. Cai, J. A. Schuller, S. Fan, and M. L. Brongersma, *Nano Lett.* **10**, 439 (2010).
61. M. D. Kelzenberg, D. B. Turner-Evans, B. M. Kayes, M. A. Filler, M. C. Putnam, N. S. Lewis and H. A. Atwater, *Nano Lett.* **8**, 710 (2008).
62. B. Tian, X. Zheng, T. J. Kempa, Y. Fang, N. Yu, G. Yu, J. Huang and C. M. Lieber, *Nature* **449**, 885 (2007).
63. B. Tian, T. J. Kempa, C. M. Lieber, *Chem. Soc. Rev.* **38**, 16 (2009).
64. J. Zhu, Z. Yu, G. F. Burkhard, C. Hsu, S. T. Connor, Y. Xu, Q. Wang, M. McGehee, S. Fan and Y. Cui, *Nano Lett.* **9**, 279 (2009).
65. C. Hsu, S. T. Connor, M. X. Tang and Y. Cui, *Appl. Phys. Lett.* **93**, 133109 (2008).
66. K. Peng, X. Wang, L. Li, X. Wu and S. Lee, *J. Am. Chem. Soc.* **132**, 6872 (2010).
67. O. El Daif, E. Drouard, G. Gomard, A. Kaminski, A. Fave, M. Lemiti, S. Ahn, S. Kim, P. Rocai Cabarrocas, H. Jeon and C. Seassal, *Opt. Express* **18**, A293 (2010).
68. L. Zeng, P. Bermel, Y. Yi, B. A. Alamariu, K. A. Broderick, J. Liu, C. Hong, X. Duan, J. Joannopoulos and L. C. Kimerling, *Appl. Phys. Lett.* **93**, 221105−221105-3 (2008).
69. R. Biswas, J. Bhattacharya, B. Lewis, N. Chakravarty and V. Dalal, *Solar Energy Mater. Solar Cells* **94**, 2337 (2010).
70. B. Curtin, R. Biswas and V. Dalal, *Appl. Phys. Lett.* **95**, 231102−231102-3 (2009).
71. J. Mertz, *J. Opt. Soc.Am. B* **17**, 1906 (2000).
72. D. M. Schaadt, B. Feng and E. T. Yu, *Appl. Phys. Lett.* **86**, 063106 (2005).
73. Y. A. Akimov and W. S. Koh, *Nanotechnology* **21**, 235201 (2010).
74. P. Matheu, S. H. Lim, D. Derkacs, C. McPheeters and E. T. Yu, *Appl. Phys. Lett.* **93**, 113108 (2008).
75. D. Derkacs, W. V. Chen, P. M. Matheu, S. H. Lim, P. K. L. Yu, E. T. Yu, *Appl. Phys. Lett.* **93**, 091107 (2008).
76. F. Hallermann, C. Rockstuhl, S. Fahr, G. Seifert, S. Wackerow, H. Graener and G. V. Plessen and F. Lederer, *Phys. Status Solidi* (*A*) **205**, 2844 (2008).
77. S. Pillai, K. R. Catchpole, T. Trupke and M. A. Green, *J. Appl. Phys.* **101**, 093105 (2007).
78. F. J. Beck, A. Polman and K. R. Catchpole, *J. Appl. Phys.* **105**, 114310 (2009).
79. H. Mertens, J. Verhoeven, A. Polman and F. D. Tichelaar, *Appl. Phys. Lett.* **85**, 1317 (2004).
80. G. Xu, M. Tazawa, P. Jin, S. Nakao and K. Yoshimura, *Appl. Phys. Lett.* **82**, 3811 (2003).
81. F. J. Beck, S. Mokkapati, A. Polman and K. R. Catchpole, *Appl. Phys. Lett.* **96**, 033113 (2010).
82. S. Mokkapati, F. J. Beck, A. Polman and K. R. Catchpole, *Appl. Phys. Lett.* **95**, 053115 (2009).
83. S. E. Han and G. Chen, *Nano Lett.* **10**, 1012 (2010).
84. S. E. Han and G. Chen, *Nano Lett.* **10**, 4692 (2010).
85. J. Li, H. Yu, S. M. Wong, G. Zhang, X. Sun, P. G. Lo and D. Kwong, *Appl. Phys. Lett.* **95**, 033102 (2009).
86. J. Li, H. Yu, S. M. Wong, X. Li, G. Zhang, P. G. Lo and D. Kwong, *Appl. Phys. Lett.* **95**, 243113 (2009).
87. Y. Park, E. Drouard, O. E. Daif, X. Letartre, P. Viktorovitch, A. Fave, A. Kaminski, M. Lemiti and C. Seassal, *Opt. Express* **17**, 14312 (2009).
88. X. Sheng, S. G. Johnson, J. Michel and L. C. Kimerling, *Opt. Express* **19**, A841 (2011).
89. V. E. Ferry, A. Polman and H. A. Atwater, *ACS Nano* **5**, 10055 (2011).
90. A. Taflove, *IEEE Transact. Electromagnetic Compatibility EMC* **22**, 191 (1980).
91. K. Yee, *IEEE Transact. Antennas and Propagation* **14**, 302 (1966).
92. J. Berenger, *J. Comput. Phys.* **114**, 185 (1994).
93. E. Yablonovitch, *J. Opt. Soc. Am.* **72**, 899 (1982).
94. P. Sheng, *IEEE Transact. Electron Devices* **31**, 634 (1984).
95. P. Bermel, C. Luo, L. Zeng, L. C. Kimerling and J. D. Joannopoulos, *Opt. Express* **15**, 16986 (2007).
96. S. Zanotto, M. Liscidini and L. C. Andreani, *Opt. Express* **18**, 4260 (2010).
97. D. Zhou and R. Biswas, *J. Appl. Phys.* **103**, 093102 (2008).
98. A. Chutinan, N. P. Kherani and S. Zukotynski, *Opt. Express* **17**, 8871 (2009).
99. L. Zeng, Y. Yi, C. Hong, J. Liu, N. Feng, X. Duan, L. C. Kimerling and B. A. Alamariu, *Appl. Phys. Lett.* **89**, 111111 (2006).

100. N. Feng, J. Michel, L. Zeng, J. Liu, C. Hong, L. Kimerling and X. Duan, *IEEE Transact. Electron Devices* **54**, 1926 (2007).
101. P. G. O'Brien, N. P. Kherani, A. Chutinan, G. A. Ozin, S. John and S. Zukotynski, *Adv. Mater.* **20**, 1577 (2008).
102. A. Centeno, J. Breeze, B. Ahmed, H. Reehal and N. Alford, *Opt. Lett.* **35**, 76 (2010).
103. K. R. Catchpole and S. Pillai, *J. Appl. Phys.* **100**, 044504 (2006).
104. K. R. Catchpole and A. Polman, *Opt. Express* **16**, 21793 (2008).
105. W. Wang, S. Wu, K. Reinhardt, Y. Lu and S. Chen, *Nano Lett.* **10**, 2012 (2010).
106. R. A. Pala, J. White, E. Barnard, J. Liu and M. L. Brongersma, *Adv. Mater.* **21**, 3504 (2009).
107. S. Fahr, T. Kirchartz, C. Rockstuhl and F. Lederer, *Opt. Express* **19**, A865 (2011).
108. J. Gjessing, A. S. Sudboã and E. S. Marstein, *J. Appl. Phys.* **110**, 033104 (2011).
109. F. Wang, H. Yu, J. Li, S. Wong, X. W. Sun, X. Wang and H. Zheng, *J. Appl. Phys.* **109**, 084306 (2011).
110. F. Wang, H. Yu, J. Li, S. Wong, X. W. Sun, X. Wang and H. Zheng, *J. Appl. Phys.* **109**, 084306 (2011).
111. Q. G. Du, C. H. Kam, H. V. Demir, H. Y. Yu, and X. W. Sun, *Opt. Lett.* **36**, 1713 (2011).
112. C. Lin and M. L. Povinelli, *Opt. Express* **17**, 19371 (2009).
113. C. Lin and M. L. Povinelli, *Opt. Express* **19**, A1148 (2011).
114. H. Bao and X. Ruan, *Opt. Lett.* **35**, 3378 (2010).
115. B. Wang and P. W. Leu, *Nanotechnology* **23**, 194003 (2012).
116. L. Cao, J. S. White, J. Park, J. A. Schuller, B. M. Clemens and M. L. Brongersma, *Nat. Mater.* **8**, 643 (2009).
117. X. Li, N. P. Hylton, V. Giannini, K. Lee, N. J. Ekins-Daukes and S. A. Maier, *Opt. Express* **19**, A888 (2011).
118. M. J. Kerr and A. Cuevas, *Semiconductor Sci. Technol.* **17**, 35 (2002).